Compact and sensitive heterodyne receiver at 2.7 THz exploiting a quasi-optical HEB-QCL coupling scheme

F. Joint, G. Gay, P.-B. Vigneron, T. Vacelet, S. Pirotta, R. Lefevre, Y. Jin, L. H. Li, A. G. Davies, E. H. Linfield, et al.

Applied Physics Letters

Compact and sensitive heterodyne receiver at 2.7 THz exploiting a quasi-optical HEB-QCL coupling scheme

Cite as: Appl. Phys. Lett. **115**, 231104 (2019); https://doi.org/10.1063/1.5116351
Submitted: 25 June 2019 . Accepted: 15 November 2019 . Published Online: 04 December 2019

F. Joint, G. Gay, P.-B. Vigneron, T. Vacelet, S. Pirotta, R. Lefevre, Y. Jin, L. H. Li, A. G. Davies, E. H. Linfield, Y. Delorme, and R. Colombelli

Applied Physics Letters ARTICLE scitation.org/journal/apl

Compact and sensitive heterodyne receiver at 2.7 THz exploiting a quasi-optical HEB-QCL coupling scheme

Cite as: Appl. Phys. Lett. **115**, 231104 (2019); doi: 10.1063/1.5116351
Submitted: 25 June 2019 · Accepted: 15 November 2019 ·
Published Online: 4 December 2019

F. Joint,[1,2] G. Gay,[1] P.-B. Vigneron,[2] T. Vacelet,[1] S. Pirotta,[2] R. Lefevre,[1] Y. Jin,[2] L. H. Li,[3] A. G. Davies,[3] E. H. Linfield,[3] Y. Delorme,[1,a)] and R. Colombelli[2,b)]

AFFILIATIONS

[1]LERMA, Observatoire de Paris, PSL Research University, CNRS, Sorbonne Universites, UPMC University Paris 06, F-75014 Paris, France
[2]Centre de Nanosciences et de Nanotechnologies (C2N), CNRS UMR 9001, University Paris-Sud, Université Paris-Saclay, 91120 Palaiseau, France
[3]School of Electronic and Electrical Engineering, University of Leeds, Leeds LS2 9JT, United Kingdom

[a)]E-mail: yan.delorme@obspm.fr
[b)]E-mail: raffaele.colombelli@u-psud.fr

ABSTRACT

We demonstrate a sensitive and compact terahertz heterodyne detection system based on a quantum cascade laser (QCL) as a local oscillator and a hot electron bolometer (HEB) as a mixer. It relies on an original optical coupling scheme where the terahertz (THz) signal to be detected and the local oscillator (LO) signal are coupled to the HEB from both sides of the integrated lens/antenna mixer. The THz signal of interest impinges on the front side through the silicon lens while the LO onto the rear (air) side. This concept allows us to remove the beam splitter usually employed in terahertz heterodyne receivers. The mixer consists of a Niobium Nitride HEB with a log-spiral planar antenna mounted on the flat side of a hyperhemispherical silicon lens. The local oscillator of the heterodyne detector is a low power consumption and low beam divergence 3rd-order distributed feedback laser with single mode emission at the target frequency of 2.7 THz. The coupling between the QCL and the HEB has been further optimized, using a dielectric hollow waveguide that reliably increases the laser beam directivity and permits us to pump the HEB into its most sensitive state through the air side of the planar antenna. We have measured a noncorrected double sideband receiver noise temperature of 880 K at 2.7 THz.

The study of the interstellar medium and its role in galaxy evolution has advanced thanks to the continuous increase in sensitivity and frequency resolution of the far-infrared (FIR) and submillimeter heterodyne receivers, as demonstrated by the space and ground based observatories such as Herschel, ALMA, or SOFIA.[1–6] Frequencies beyond 2 THz are of particular interest, especially for the spectroscopy of the rotational transition lines of HD, NH_3, and H_2O.[7]

The first key element of a terahertz heterodyne detector is the nonlinear mixer that down converts the terahertz signal into lower frequencies for signal processing. Superconducting hot electron bolometers (HEBs) are good candidates for detecting weak signals in the THz range. Such heterodyne detectors require radiant power from a local oscillator (LO)—the second key element to achieve the mixing process. The THz and LO signals are usually coupled to the mixer using a diplexer or a beam splitter. Terahertz quantum cascade lasers (QCLs) are promising semiconductor laser sources operating above 1.5 THz with output powers in the milliwatt range.[8] The combination of a QCL as LO and an HEB as a mixer represents an attractive THz heterodyne detection system that is currently employed in missions for astronomical observations.[9] For future space missions, further developments are, however, necessary to improve the integration of QCL-based LOs with HEBs to reach higher compactness, lower QCL power dissipation, and better power coupling between QCL and HEB.

In this letter, we present a solution that addresses the aforementioned issues by simplifying the heterodyne measurement scheme. An original optical coupling scheme is demonstrated where the LO is coupled through the air side of the planar HEB antenna, while the signal to be detected is coupled to the HEB through the lens, as in conventional quasi-optical detection systems. An extremely low double sideband receiver noise temperature of 880 K at an operating frequency of

2.7 THz is obtained, confirming the potential for ultrahigh sensitive heterodyne detection of this scheme.

The main requirements for a THz QCL as LO in a heterodyne system are (i) single frequency operation, (ii) low-power consumption, and (iii) good output beam quality. The latter ensures optimal coupling into the mixer. These requirements can be satisfied by a variety of approaches: photonic crystals,[10,11] surface-emitting lasers,[12,13] "plasmonic" lasers,[14] terahertz VECSELs,[15] patch array antenna lasers,[16] and first or third order distributed feedback (DFB) lasers.[9,17] For low power dissipation, the latter approach is extremely competitive as such devices can be made very small (i.e., low power consumption) without compromising the output beam quality. A difficulty remains in obtaining a precisely predefined emission frequency and simultaneously an optimal beam pattern, as both are controlled by the same parameter: the effective index n_{eff}. Using the definition of the effective index proposed in Ref. 18: $n_{eff} = 3\lambda_0/2\Lambda$, with Λ being the grating period, the optimal far-field is obtained when $n_{eff} = 3$. Departing from this condition that assures constructive interference in the far-field, for example, by attempting to implement a precise emission frequency, degrades the beam profile.[17–19] In this work, we also describe a practical technique to reliably reshape the far-field emission pattern of THz frequency 3rd-order DFB lasers into near-Gaussian beams. The technique is based on dielectric hollow waveguides (HWs),[20–22] and it permits us to decouple the precise frequency selection of the LO from its output beam quality.

We have designed and implemented 3rd-order DFB gratings on metal-metal waveguide THz QC lasers with target single mode emission at $\approx 90\,cm^{-1}$ (2.7 THz). The QCL heterostructure is adapted from a bound-to-continuum design[23] with the resonant phonon assisted depopulation mechanism. It was grown with 136 periods, leading to a 15 μm thick active region. The structure—grown on a SI-GaAs wafer—consists of a 300-nm-thick GaAs buffer layer, 700 nm-thick highly doped GaAs layer followed by 136 periods of the active region, and an 80 nm-thick doped GaAs contact layer. One period has the following sequence: **3**/8.6/**3**/9.5/**3**/11.8/**2**/12.9/**1**/16.2/**0.5**/10.1/**4**/14.5/**3**/17/**3**/8.5, where the thickness is given in nanometers, and the $Al_{0.15}Ga_{0.85}As$ barriers are indicated in bold. The devices have been processed using a standard procedure for the metal-metal THz waveguide, and the lateral corrugation has been defined using inductively coupled plasma dry-etching based on $BCl_3/Cl_2\ N_2$ chemistry.[24] A SEM image of a typical device is reported in Fig. 1(a) (inset). To ensure that only the fundamental transverse mode propagates in the laser cavity and to reduce the device size, the lateral ridge width is 15 μm for the wider sections and 5 μm for the narrower sections. The grating duty cycle (DC, i.e., the ratio between the narrow section length and the grating period) permits us to control the DFB coupling constant coefficient κ that we calculate numerically. Using values of $\kappa = 43.9\,cm^{-1}$ and a total laser length of L = 800 μm, we obtain a κL value of $\sim$3.5, which ensures low threshold current and low spatial hole burning. The grating DC is also used to fine-tune the target laser frequency. To guarantee single mode operation, the photonic gap of the 3rd-order DFB has been designed to be 300-GHz-wide, thus ensuring that the band edge states of the photonic structure will not simultaneously experience elevated optical gains and only the mode at the target frequency will lase (*cf.* supplementary S3). Several DFB lasers with different DCs and periodicities were fabricated to ensure that the target frequency is attained in one fabrication run. Owing to the low

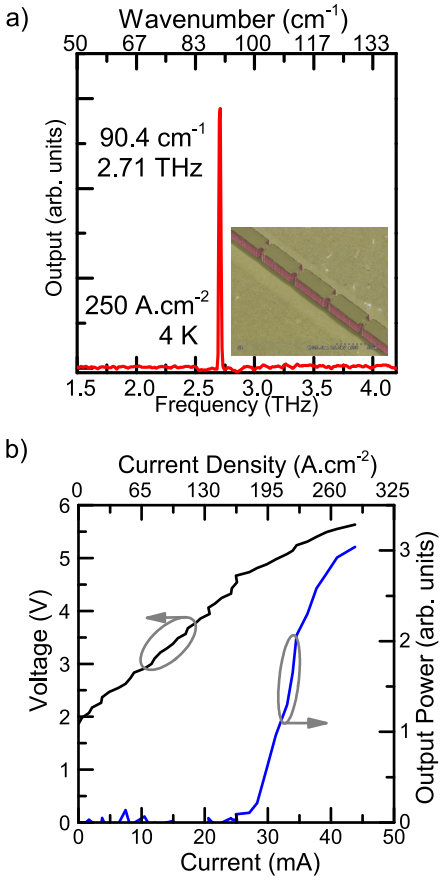

FIG. 1. (a) Emission spectrum at a temperature of 10 K for a device with a grating period of 54.8 μm. The device is operated in pulsed mode with 10 μs long pulses and (b) the corresponding light-current-voltage characteristic. The inset shows a SEM image of a typical 3rd-order terahertz DFB laser with lateral corrugations.

threshold current density of the L1395 material, both pulsed and continuous wave (CW) laser operations were achieved. Lasing was observed up to 90K in pulsed operation. Figure 1(a) shows a typical single-mode laser spectrum at the target frequency with a duty cycle of 90% (pulsed duration 1 μs; repetition rate 90 kHz). The operating currents of such lasers are in the 30–50 mA range only, owing to the reduced device surface area [Fig. 1(b)]. The power dissipation is $<$200 mW, thus enabling an ultracompact integration of the devices with the HEB mixer. At the lowest temperature (4 K), a maximum output power of 850 μW has been measured in continuous wave (CW) with a Thomas Keating absolute THz power meter.

The 3rd-order grating selects the laser frequency and also enables light extraction into free space. If the effective index of the lasing mode is exactly $n_{eff} = 3$, photons diffracted from each corrugation constructively interfere, forming a narrow output beam at a small angle from the horizontal direction [Fig. 2(a)].[17] The experimentally measured beam pattern of a laser achieving such a phase matching condition is presented in Fig. 2(b). The laser waveguide comprises 14 grating periods with a periodicity of $\Lambda = 54.8\ \mu m$ so that the Bragg frequency matches the target of 2.7 THz. The grating DC is 12%. The full width at half

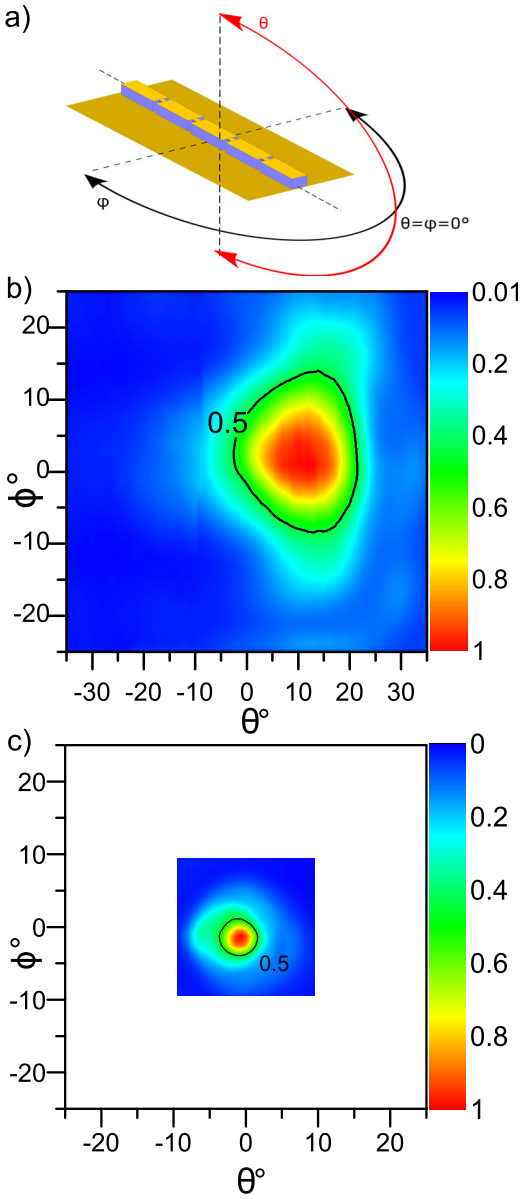

FIG. 2. (a) Schematic diagram showing the scanning angles used in the far-field measurements. (b) Typical far-field beam pattern obtained from a perfectly phase matched 2.7 THz 3rd-order DFB QCL measured 11 cm away from the center of the laser. (c) The corresponding far-field beam pattern for the same 3rd-order DFB QCL measured with the HW connected to the laser facet taken 11 cm away from the end aperture of the HW.

maximum (FWHM) of the measured beam-pattern is 20° in both θ and ϕ planes with a directivity of 20 dBi. However, such a type of beam pattern is not the norm for 3rd-order THz QCLs as perfect phase matching is hard to achieve. The beam pattern is often more divergent, and it does not always have a regular profile. We have investigated different strategies to improve the QCL output beam shape to optimize the power coupling with the mixer. One interesting solution is the use of dielectric HWs to reshape the beam pattern of nonphase matched 3rd-order DFBs and further increase the beam directivity to case both QCL and HEB in the same cryostat for compactness purposes.

A dielectric HW is an over-sized waveguide whose hollow core diameter is much larger than the wavelength of the radiation (λ_0). It consists of a cylindrical hollow core of radius a, surrounded by a higher refractive index reflective wall (we use Pyrex, $n_{Pyrex} = 1.474$). Marcatili[25] has determined the field distribution and propagation constants of the first few eigenmodes. The structure supports three types of modes: transverse circular electric (TE_{ij}), transverse circular magnetic (TM_{ij}), and hybrid modes (HE_{ij}) where all the electric and magnetic components are present. The latter mode is the one of interest for our application. The attenuation constants of these modes are proportional to λ_0/a^3: if λ_0 is much smaller than the a, the mode overlap with the lossy Pyrex is reduced, and the propagation losses are low. In fact, the propagation losses in the HW are only 0.1 dB/m at 2.7 THz for a bore diameter of 4 mm according to the wave-optics based formula in Ref. 26.

Since the total loss depends on both propagation *and* input losses into the desired mode, it is important to couple as much light as possible into the lowest order HE_{11} mode. We have devised different strategies to couple the QCL output into the HW. The most compact solution consists in positioning the laser facet directly at one end aperture of the HW, but this technique shows high coupling loss (Fig. S1, supplementary material). In this work, we have instead focused the laser beam at the HW aperture with two small parabolic mirrors and thus improved the coupling efficiency. The first advantage of the dielectric HW is its beam shaping ability. Figure 2(c) shows the far-field emission pattern of the 3rd-order DFB laser with a 4-mm-bore-diameter dielectric HW positioned at the laser facet. Compared to its original far field pattern [Fig. 2(b)], the beam FWHM is greatly reduced to 5° × 5° in both θ and ϕ planes with a significantly enhanced directivity of 55 dBi. When combined with a nonphase matched QCL, the HW reshapes the irregular emission profile into a near circular beam with a dramatically reduced angular width as shown in Fig. S2 (supplementary material). The second advantage, of crucial interest when implementing an ultra-compact heterodyne system, is that the beam direction is now precisely predictable (it lies along the HW direction) and the *in situ* optical alignment with the HEB mixer is simplified.

The mixer consists of a superconducting HEB connected to a gold log spiral planar antenna on a high resistivity silicon lens. Its concept is described in Ref. 27, and it has been fabricated with the process developed at LERMA.[28] The ultrathin 5-nm-thick NbN film was provided by the company SCONTEL.[29] The NbN superconducting bridge is 0.2 μm long and 2 μm wide [Fig. 3(a)]. The critical temperature T_c of the superconductor is 9.2 K, and the normal state resistance of the HEB at room temperature is 75 Ω. Without incident power, the critical current I_c is 320 μA at 4.2 K. The incoming THz signal and the LO are coupled onto the superconducting bridge via the log-spiral planar antenna whose polarization, radiation pattern, and impedance are frequency independent over a large bandwidth. The HEB with its antenna is mounted on the back of a hyperhemispherical lens with an antireflection coating designed for 2.5 THz to increase the antenna directivity in the dielectric. The beam pattern of a log-spiral antenna on an extended hemispherical silicon lens has been previously calculated for a frequency of 600 GHz:[30] a FWHM of the mainlobe around 4.8° is obtained. However, at 2.7 THz, the lens is much larger than the wavelength, and it is challenging to perform a similar simulation with full wave electromagnetic solvers, as a very large amount of memory

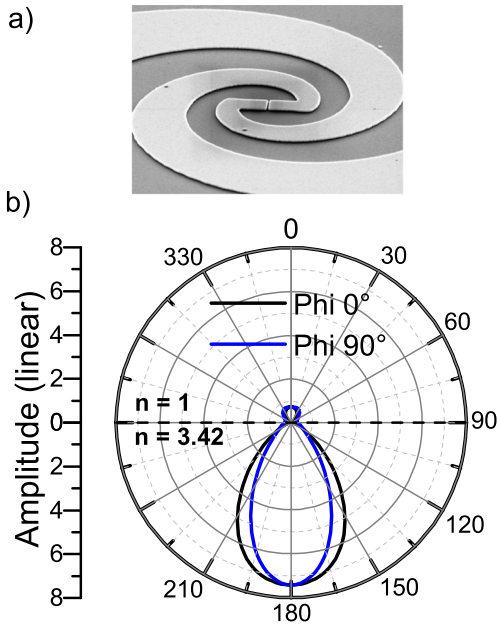

FIG. 3. (a) SEM picture of the double-helix log spiral antenna of the HEB. (b) Numerical simulation of the beam pattern of our log-spiral antenna at the interface of two infinite dielectric half spaces with index of refraction $n_{air} = 1$ for the upper half space and $n_{HR\text{-}Si} = 3.4$ (HR-Si at 2.7 THz) for the lower half space, respectively.

would be required. We obtained an estimate of the antenna radiation power distribution on both air and dielectric sides by simulating the power gain of the antenna at the interface of two infinite dielectric half spaces using the finite element solver FEKO. When the planar antenna lies at the silicon-air interface, the radiated power in the air is ten times smaller than in the dielectric [Fig. 3(b)]. However, the 3rd-order DFB THz QCL can deliver several hundred microwatts of laser power. In combination with the high directivity provided by the HW, we can efficiently couple the LO signal through the air side of the planar antenna. This original configuration permits us to remove the beam splitter usually employed, thus simplifying the optical system and making an optimal use of the weak THz input power.

The experimental setup for the double-sideband noise temperature measurement is shown in Fig. 4(a). The coupling of the THz radiant power onto the HEB was made through the hyperhemispherical Si lens. The 3rd-order QCL, the LO, was optically coupled to a 4 mm bore diameter HW with two small parabolic mirrors to maximize the power injected in the waveguide. The 20 mm long HW is mounted with its end-aperture aligned with the log spiral antenna: this permits us to easily perform this alignment. The THz QCL is operated in CW with no active stabilization, and the pumped voltage current curve of the HEB monitors the pumping level. We were able to pump the HEB into a sensitive state for a QCL bias voltage close to its maximum output power ($\sim 5.0\,V$, optical output power $\sim 850\,\mu W$). The negative resistance where the characteristic of the HEB is perturbed is suppressed. The measurements have been performed with different LO pumping levels. In Fig. S4 (supplementary material), we show the HEB's IV curves at the LO pumping level where we obtained the mixer's minimum noise temperature, with hot (red curve) and cold (black curve) loads connected to the input of the mixer, respectively.

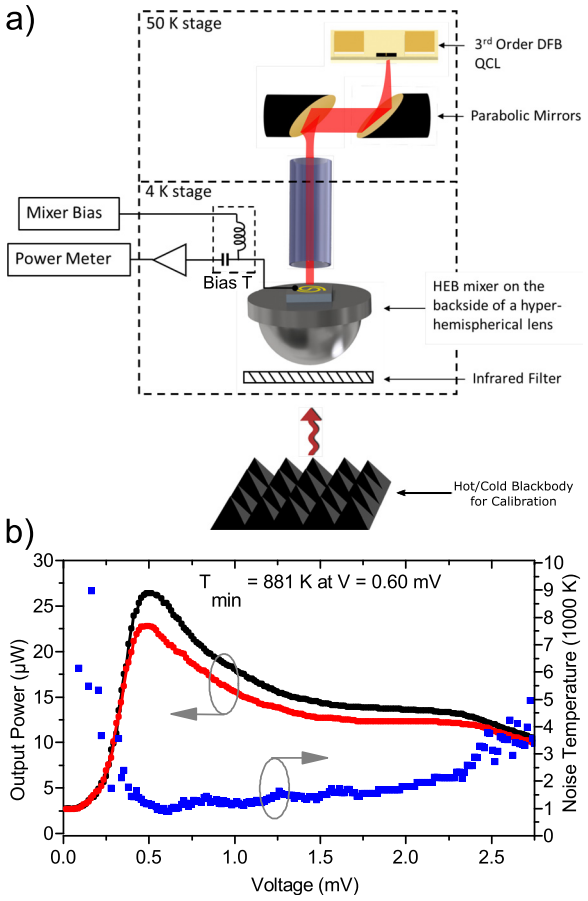

FIG. 4. (a) Experimental setup for heterodyne measurements with a compact integration of the QCL with the HEB. (b) Current-voltage characteristics of our HEB mixer with the 3rd-order DFB QCL radiation at 2.7 THz responding to the hot and cold black body placed at the input of the mixer. (c) IF output power as a function of the HEB bias voltage (black and red dots) and the corresponding receiver noise temperature T_{REC} (blue dots) measured with the Y-factor method.

The intermediate frequency (IF), resulting from the mixing of the LO and the incoming THz signal, is extracted by a coaxial cable via a bias-T and amplified by a low noise cryogenic amplifier followed by two room temperature amplifiers. The IF power with a center frequency at 1.5 GHz and a bandwidth of 100 MHz is recorded by a sub-millimeter wave range power-meter. The receiver noise temperature, the figure of merit gauging the overall system sensitivity, has been determined with the Y-factor technique. It consists in measuring the receiver IF output power when two blackbodies (hot and cold) are placed, respectively, at the receiver's input. The Y factor is given by $Y = P_{IF}(hot)/P_{IF}(cold)$, and the double sideband (DSB) receiver noise temperature is obtained using the following formula:

$$T_{rec}^{DSB} = \frac{T_{hot} - Y \times T_{cold}}{Y - 1}. \quad (1)$$

The Callen-Welton black body temperatures at 2.7 THz are $T_{cold} = 95$ K and $T_{hot} = 300$ K. We have swept the bias voltage of the HEB

and recorded for both cases (hot and cold black body) the IF output power that is presented in Fig. 4(b) (black and red dots). The resulting receiver noise temperature is calculated with Eq. (1) and is reported in Fig. 4(c) (blue dots). We have obtained the lowest noise temperature of 880 K at 2.7 THz for a HEB's applied bias voltage of 0.6 mV. This uncorrected noise temperature is relatively close to the one reported in Ref. 27 where a noise temperature of 790 K has been obtained at 2.5 THz with an optically pumped far-infrared gas laser as LO. Compared to the previous reported experiment, the advantage of the present measurement setup is the major improvement in terms of compactness, low power consumption, and, in particular, the absence of the beam splitter that permits us to maximize the transmission of the THz signal to be detected.

We have then measured the QCL beat-note against an ultrastable Amplifier Multiplier Chain (AMC) from VDI using the integrated QCL-HEB system in Fig. 4(a). Figure S5(a) (supplementary material) shows a system diagram for the beat-note measurements. A beat signal between QCL and the AMC is detected by the HEB mixer with an IF frequency of 2.530 GHz, whose power spectrum (with the free-running QCL) is reported in Fig. S5(b) (supplementary material) with a FWHM of ∼117 kHz. The low-frequency jitter we measure indicates good temperature stability of the QCL and low mechanical oscillations of the cryocooler. In the future, we plan to implement the phase-lock of the QCL to further improve the receiver sensitivity. The phase-locking of a THz QCL has been demonstrated using phase locking Loop systems,[31–34] but the latest method proposed by Freeman *et al.*[35] using injection locking is possibly more attractive when considering its compact integration capacity.

In conclusion, we have demonstrated a heterodyne receiver at 2.7 THz with an original coupling scheme between the LO and the quasi-optical mixer. The LO is a 3rd-order DFB QCL, and the mixer is a superconducting NbN HEB with an integrated lens antenna. The THz signal and the LO are coupled to the HEB from both front and rear sides of the mixer, allowing the removal of the beam splitter usually employed in heterodyne measurements. The lowest measured noise temperature is 880 K, indicating a very good performance for this system that offers a better incoming radiant power transmission and a much more compact implementation (useful, for instance, for future multipixel configurations). We have also demonstrated that using a dielectric hollow waveguide, an irregular far-field profile emitted by the LO (a THz QCL in this case) can be reshaped into a near Gaussian beam with a reduced divergence and an improved directivity, thus facilitating the optical alignments with the other components. The improvements demonstrated in this work are of interest for THz coherent detections, for compact and sensitive imagery in future space missions.

See the supplementary material for the details on the compact coupling scheme with HWs; optimal coupling scheme with HWs; losses of the 3rd order DFB QCL and QCL material; DC characteristics of the HEB mixer; and QCL beat-note against an ultrastable Amplifier Multiplier Chain.

We acknowledge partial financial support from the Centre National d'Etudes Spatiales (CNES), from the European Research Council (IDEASERC) ("GEM") (No. 306661), from the EPSRC (UK) Grant HyperTerahertz (No. EP/P021859/1), and from the European Union FET- Open Grant ULTRA-QCL (No. 665158) and from the Union FET-Open Grant MIR-BOSE (737017). This work was partly supported by the French RENATECH network. EHL acknowledges the support of the Royal Society and the Wolfson Foundation. We are also very grateful for the help of Dr. Mohammed Salih in the characterization and optimization of the epitaxial material growth, Pierre Bonnay for providing us with the hollow pipes, and Laurent Pelay for the mechanical work on the copper blocks.

REFERENCES

[1]M. Harwit, Adv. Space Res. **34**, 568 (2004).
[2]A. Wootten, Large Ground-Based Telesc. **4837**, 110 (2003).
[3]S. Heyminck *et al.*, Astron. Astrophys. **542**, L1 (2012).
[4]C. Risacher *et al.*, in International Conference on Infrared, Millimeter, Terahertz Waves, IRMMW-THz (2014), pp. 1–2.
[5]E. T. Young *et al.*, Astrophys. J. Lett. **749**, L17 (2012).
[6]C. Risacher *et al.*, J. Astron. Instrum. **7**, 1840014 (2018).
[7]B. J. Drouin *et al.*, J. Mol. Struct. **1006**, 2 (2011).
[8]R. Köhler *et al.*, Nature **417**, 156–159 (2002).
[9]H. Richter *et al.*, IEEE Trans. Terahertz Sci. Technol. **5**, 539 (2015).
[10]C. Sirtori *et al.*, Nat. Photonics **7**, 691 (2013).
[11]Y. Chassagneux *et al.*, Nature **457**, 174 (2009).
[12]G. Xu *et al.*, Nat. Commun. **3**, 952 (2012).
[13]J. A. Fan *et al.*, Opt. Express **14**, 11672 (2006).
[14]C. Wu *et al.*, APL Photonics **2**, 026101 (2017).
[15]L. Xu *et al.*, Appl. Phys. Lett. **107**, 221105 (2015).
[16]L. Bosco *et al.*, Appl. Phys. Lett. **109**, 201103 (2016).
[17]M. I. Amanti *et al.*, Nat. Photonics **3**, 586 (2009).
[18]T.-Y. Kao *et al.*, Opt. Lett. **37**, 2070 (2012).
[19]T.-Y. Kao *et al.*, Opt. Express **23**, 17091 (2015).
[20]R. Degl'Innocenti *et al.*, Opt. Express **22**, 24439 (2014).
[21]A. A. Danylov *et al.*, Appl. Opt. **46**, 5051 (2007).
[22]P. Patimisco *et al.*, Sensors **13**, 1329 (2013).
[23]M. Wienold *et al.*, Electron. Lett. **45**, 1030 (2009).
[24]P. B. Vigneron *et al.*, Microelectron. Eng. **202**, 42 (2018).
[25]E. A. J. Marcatili and R. A. Schmeltzer, Bell Syst. Tech. J. **43**, 1783 (1964).
[26]J. J. Degnan, Appl. Phys. **11**(1), 1 (1976).
[27]Y. Delorme *et al.*, in 22nd International Symposium on Space Terahertz Technology, ISSTT (2011), pp. 123–126.
[28]R. Lefèvre *et al.*, in 23rd International Symposium Space on Terahertz Technology, ISSTT (2012), pp. 122–125.
[29]See http://www.scontel.ru/ for the web address of the company.
[30]W. Miao *et al.*, in Proceedings of the 8th International Symposium on Antennas, Propagation EM Theory, ISAPE (2008), pp. 58–61.
[31]D. Rabanus *et al.*, Opt. Express **17**, 1159 (2009).
[32]P. Khosropanah *et al.*, Opt. Lett. **34**, 2958 (2009).
[33]S. Barbieri *et al.*, Nat. Photonics **4**, 636 (2010).
[34]A. Danylov *et al.*, Opt. Lett. **40**, 5090 (2015).
[35]J. R. Freeman *et al.*, Optica **4**, 1059 (2017).